

FEDSM2003-45242

THE VELOCITY FIELD OF AN ANNULAR JET WITH "CROSS-MEMBER"

John F. Foss, Professor
Richard J. Prevost, Graduate Research Assistant
Kyle M. Bade, Research Assistant
Aurélien Levasseur, Visiting Research Assistant

Michigan State University
Mechanical Engineering Department
East Lansing, Michigan, 48824

ABSTRACT

An annular jet has been created by supporting a streamlined plug (dia= D_1) in a delivery tube (dia= D_2) with a narrow cross-member. PIV measurements have been carried out at $x/D_2=8$ for four D_1/D_2 ratios. These observations, and the motivating criteria for this study, were used to select $D_1/D_2=0.746$ for detailed, near exit, velocity field measurements. Significant three-dimensional effects of the cross-member have been observed. Velocity field data, from a "sting supported, flat disk" (axisymmetric geometry) central plug provide comparative measurements. These comparisons are considered in detail.

Keywords: *Annular Jet, PIV*

NOMENCLATURE

D_1, R_1 annulus inner diameter, inner radius
 D_2, R_2 annulus outer diameter, outer radius
 Q flow rate, see Fig. 3
 R_e see Eq. (1c) and, (3)
 U_o characteristic velocity, see Eq. (1b)
 \vec{V}, u_x, u_r See Eq. (2)
 \vec{V}, u, v, w See Eq. (4)
 r see Fig. 3, $r^*=r/R_2$
 x, y, z see Fig. 7, $x^*=x/R_2$, etc.
 $(\bar{\quad}), (\quad)', (\tilde{\quad})$ ensemble mean, fluctuating and rms values of (\quad)

INTRODUCTION

The present investigation of the annular jet geometry is motivated by the authors' interest in developing a "spot cooling" axial fan. Such fans would be used, for example, in a manufacturing assembly line, a foundry, a bakery, or livestock holding facility where a directed jet of cooling air would benefit the comfort and productivity of the target person/animal. The benefits of spot cooling workers, in a relatively high temperature environment as noted above, can be intuitively appreciated. These benefits are also supported by published references. For example, Rohles [1] and Rohles, et al. [2] have considered the "effective temperature" and other ways to characterize personal comfort.

The benefits of spot cooling for dairy cattle can be even more strongly supported. Increased air velocity over the body surface of a dairy cow and the resultant increased convective heat and mass transfer can offset some of the negative effects of hot weather (Brody, et al. [3]). With the high levels of milk production possible today with improved breeding, feeding, management and facilities, the cows' need to dissipate metabolic heat is substantially increased (Tyrrell, et al. [4]); (Tillotson and Bickert [5]). Using fans to increase air velocity in the vicinity of the cow during hot weather has been found to be an important asset (Chastain [6]).

This investigation is a preliminary step in such a development and its hypothesis is that a large hub region will create a significant reverse flow region and an initial narrowing of the outer stream surface such that the downstream axisymmetric jet will appear to originate at a substantial distance downstream of the fan plane. This is important since the actual fan will be placed at nominally 8 diameters from the target object for the "spot cooling".

The idealized geometry of the present study, that is to be representative of the axial fan flow, is shown in Fig. 1. A delivery tube of diameter D_2 brings air from a pressurized plenum to the exit plane. A cross-member supports the central elliptical-nose obstruction (diameter D_1) that would represent the drive motor in the application problem. In addition to the stated motivation, the present study also contributes to the quite limited body of knowledge regarding the development of a jet exhausting from "a modified" annular exit as studied herein. The modification: a single cross-member supporting the central plug, is a mechanically simple technique to create the annulus.

It can be explicitly noted that the present jet study will not attempt to mimic the swirl component that would result from a fan flow without stators. The presence of swirl is known to induce enhanced entrainment and hence it represents a deleterious effect for the intended application. Downstream stators can be employed to minimize this negative aspect of the fan flow.

An initial effort in the present investigation examined the effect of the diameter ratio: (D_1/D_2) , on the volume flux and the jet diameter at $x/D_2=8$. These results, presented in the third section, led to the diameter ratio selection of $D_1/D_2=0.757$ for the further observations.

The following sections of this communication provide a review of the relevant literature, a description of the present experimental flow facility and the PIV measurement techniques, and the results and discussion of the present observations.

LITERATURE REVIEW

The term "annular jet", can be understood to mean a central and a surrounding jet. This configuration, also referred to as a "co-axial jet", is not relevant to the present communication. The relevant studies, those of Durao and Whitelaw [7], Ko and Chan [8, 9], Kuhlman [10] and Patte-Rouland, et al. [11], have been examined for information that can give guidance to the present study.

The nozzle geometry utilized by Ko and Chan, with its inward directed annular flow at $x=0$, is rational for their intent to examine the flow fields of stabilized flames. However, it does represent a distinctly different initial condition with respect to that of the present study. These references were also executed with hot-wire probes and the authors adopted processing methods which attempted to properly interpret the rectified signal provided by these sensors. (The issue of flow disturbances, resulting from the probe shaft, was not addressed). For these reasons, the Ko and Chan investigations will not be further considered in the interpretation of the present observations.

One geometry, of the several investigated by Kuhlman [10], is relevant to the present study: his "flat topped" centered obstruction with his "flush" condition. (One caution in reading the Kuhlman paper, apparently "centerline" is meant to indicate

the radial position of: $r=[(D_1/2)+(D_2-D_1)/4]$, near the jet exit (see his Fig. 5b), and not the centerline of the axisymmetric configuration. "Centerline" regains its conventional meaning for larger x values. Kuhlman's diameter ratio: $D_1/D_2=0.75$, is satisfyingly close to the primary configuration studied herein (0.746). His data also show that the axisymmetric jet behavior, i.e., maximum velocity at $r=0$, is recovered by $x/D_{eff}=4$ where D_{eff} is given by his equation (1). This equation incorporates the compressible flow characteristics of his study, and for that reason, it will not be adopted herein. It is, however, apparent from his Figs. 2a and 3a that $x/D_{eff}=4$ is nominally $x/D_2=2.5$. The recovery of the axisymmetric jet behavior at this location in Kuhlman will be shown to be similar to that experienced in the present investigation.

Durao and Whitelaw [7] examined an annular jet whose geometry, in their words, closely resembled... "flame stabilizers used, for example in small furnaces". (See p. 370 of that reference). Their study of this fully axisymmetric configuration involved 3 diameter ratios with the largest (14.2 mm/20 mm) or $(D_1/D_2=0.71)$ receiving the most attention. In addition, their investigation was specifically focused on providing detailed flow field data (LDV) for the support of turbulence models that could be used to refine the CFD simulations of this flow field. These authors selected an "equivalent diameter using the annular jet area" for their Reynolds number. It is inferred that this definition yields:

$$D_{equiv} = [D_2^2 - D_1^2]^{1/2}, \quad (1a)$$

which, along with the characteristic velocity:

$$U_o = [2(p_p - p_{atm}) / \rho]^{1/2}, \quad (1b)$$

establishes the Reynolds number as:

$$R_e = U_o D_{equiv} / \nu. \quad (1c)$$

Their nominally similar D_1/D_2 ratio (0.71), with respect to that of the present study, and their range of exiting velocity magnitudes: U_o , provided $3.5 \leq R_e \times 10^3 \leq 28.3$ in comparison to $R_e = 23.2 \times 10^3$ for the present study. The "bluff disc" of their study is in distinct contrast to the elliptical nose obstruction of the present study. The separation stream surface, from the $r=D_1/2$ perimeter, will necessarily follow an initial trajectory described as:

$$\vec{V} = \hat{i}u_x + \hat{r}u_r \quad (2)$$

and

$$u_r > 0$$

in their investigation. In contrast, the similarly defined initial

trajectory will be $\vec{V} = \hat{u}_x$ for the present study. More importantly, their geometry is fully axisymmetric, without a cross-member, in contrast with that reported herein. Detailed comparisons are, however, useful and these are given in the results portion of the fourth section.

The Patte-Rouland, et al. [11] study is characterized by a quite large diameter ratio: $D_1/D_2=0.905$. The axisymmetric nozzle geometry for this study is not well defined in their paper. Comparative observations with the present study are presented in the results and discussion portion of the fourth section.

THE INITIAL PROGRAM

Experimental Facility

The basic flow system is shown in Fig. 2. Note that the PIV seed is introduced into the large plenum below the exit plane. The associated PIV measurements were made with a Dantec Flow Map 2000 system. Figure 4 presents the details of the interchangeable plug support which allowed four different (D_1/D_2) values to be readily examined in the initial surveys. The width (δz) of the cross-member support was: $\delta z = 0.104 R_2$, for this initial configuration. The plugs were formed with an elliptical nose that terminated at the cross-member for the initial study. The ellipse is described by the ratio of the maximum radius to the length of the (one-sided) ellipsoid. This ratio was nominally 0.28 for the four plugs that were used in the Initial Program. The interrogated regions for the initial study are shown in Figs. 2 and 3.

The jet exit plane Reynolds number,

$$Re(\text{initial study}) = U_o(R_2 - R_1)/\nu \quad (3)$$

was a variable for these initial studies since both U_o and $(R_2 - R_1)$ changed for the measurements. The Re values are stated in the next section.

As is standard with PIV, the data were derived from a set of dual pulse images (500 for each plug in these experiments) separated by a short elapsed time: Δt . A value of $\Delta t = 60 \mu\text{sec}$ was used for the near exit data where $\Delta t U_o / D_2 \approx 0.013$. In contrast, $\Delta t = 175 \mu\text{sec}$ at the $x/D_2 = 8$ location. This longer delay was selected to represent the lower velocity magnitudes at this downstream location. The ensemble of these observations can be used to create the average velocity field in the indicated plane. Note that the resolved \vec{V} in this case is $\vec{V} = \hat{u}_x + \hat{r}_r$ and that the non-dimensional average velocities: $\bar{u}_r^*(x, r, \theta = 0, \pi)$ as well as $\bar{u}_x^*(x, r, \theta = 0, \pi)$ can be used to identify the streamline pattern near the jet exit.

Experimental Results to Identify the Effect of the R_1/R_2 Ratio

The effect of the radius ratio: R_1/R_2 , was assessed by examining four separate values:

$$R_1/R_2 = 0.503, 0.637, 0.757, \text{ and } 0.857$$

with their respective Reynolds numbers (as defined by Eq. (3)):

$$Re = 6866, 5162, 3365, 1975.$$

PIV measurements were made in the near and far field: $0 \leq x^* \leq 2.5$ and $12 \leq x^* \leq 16.2$ respectively, for each of these geometries.

A representative ensemble averaged flow pattern near the jet exit is provided in Fig. 5 for the condition: $R_1/R_2 = 0.757$. The asymmetric nature of this velocity field may be in response to geometric imperfections. The general features of the image are, however, similar to those of the Patte-Rouland, et al. [11] study where the "centered" saddle point is at $x^* \approx 1.42$ for the present study and at $x^* \approx 1.0$ for that investigation. Similarly, the distinct vortex "cores" were located at $x^* \approx 0.95$ and $r^* \approx \pm 0.5$, (see Fig. 5). These same features in the PIV image of [11] were located at $x^* \approx 0.48$ and $r^* \approx \pm 0.58$. These differences may reflect the (D_1/D_2) differences or the lack of axisymmetry in the present study. The lower rhs portion of the image is inaccessible given the shadow created by the plug's support member. Similar images were obtained for the other three R_1/R_2 ratios.

A separate set of experiments was executed to identify the four, time average, velocity fields in the neighborhood of $x/D_2 = 8$. Figure 6 presents these four $u_x^*(r^*)$ distributions. The choice of $[Q_0/\pi R_2^2]$ in the definition of u_x^* , as identified in Fig. 3, was made to permit a common scaling for the four geometries. (The subsequent study of the $R_1/R_2 = 0.746$ geometry makes use of U_o as the scaling velocity.) Included with the velocity profiles are the inferred flow rates at $x/D_2 = 8$ and the jet-width measures: $[R_{1/2}/R_2]$. The definition of $R_{1/2}$ is such that $u_x^*(r=R_{1/2})/u_x^*(r=0) = 0.5$.

The quantitative measures shown in Fig. 6 can be used to identify the $R_1/R_2 = 0.757$ configuration as the best performer of the four configurations. "Best performer" is based upon the narrowest jet column and satisfactory Q_8/Q_0 .

NEAR EXIT MEASUREMENTS FOR THE SELECTED GEOMETRY

Since the initial measurements provided the clear result

that, of the geometries examined, the 0.757 diameter ratio case provided the "geometry of choice", a new (larger and more streamlined) plug was developed ($D_1/D_2=0.746$); see Fig. 7 for its specific features. This new geometry, and the additional measurement planes, prompted a new coordinate system: x,y,z cf. x,r . These coordinates are included with the geometric description of the new nozzle. This new coordinate system designation is accompanied by the velocity designation as

$$\vec{V} = \hat{i}u + \hat{j}v + \hat{k}w. \quad (4)$$

The processed data also represent the Reynolds decomposition as $u(t) = \bar{u} + u'$, etc. and \bar{u} as an rms value.

The Reynolds number for these data was 23.2×10^3 using U_o and D_{equiv} . PIV measurements were again obtained but a "next generation" system from LaVision (FlowMaster 2S Planar PIV system) was now employed. This 2Kx2K and 12-bit gray level camera was able to resolve more of the detailed features of the near field. The other aspects of the experimental configuration were unchanged.

Two orientations were examined using this planar PIV system: i) an image plane that is normal to the cross-member ($x-y$ plane), and ii) an image plane that is centered upon the support member ($x-z$ plane). These are referred to as the "perpendicular" and the "aligned" orientations. Ensemble data sets of 500 image pairs were obtained for each of the two light sheet orientations. Figures 8 and 9 present the ensemble averaged velocity field magnitudes and the associated streamline patterns for the perpendicular and aligned orientations respectively. The lower portion: $x^* \leq 0.15$, of Fig. 8 has been cropped to remove the spurious values caused by the laser glare from the annulus. This operation was not required for the aligned view given the solid (and flat black) surface in that view. It is of interest to note the significant differences between the perpendicular and the aligned velocity fields in this $0 \leq x^* < 2.5$ domain.

Specifically, the perpendicular condition (the $x-y$ plane) shows the expected high speed regions of the exiting jet (white) and the strongly accelerated ambient fluid (see the streamlines that enter the jet column from the blue to the green regions)¹. The interior region ($x-y$ plane) reveals: i) the strongly "pumped" fluid immediately aft of the plug, ii) the centered nodal point ($x^* \approx 1.2$) that demarcates the recirculation from the streamwise flows and iii) the compact "vortex motions" that are centered at (nominally) $x^* \approx 0.9$ and $y^* \approx \pm 0.5$ in this view.

The axisymmetric annular plug ($D_1/D_2=0.95$) geometry of the Patte-Rouland, et al. [11] study exhibits a distinctly different pattern. Namely their data show a centered saddle point at

$x^* \approx 1.0$ for their two Re values: 18,360 and 68,840, (as defined by Eq. (1c)). The Two vortex motions in [11] essentially occupy the domain: $0 \leq r/R_1 \leq 1$ with the centers (in the planar image) at $x^* \approx 0.48$ and $r^* \approx \pm 0.58$.

There are substantial differences between the "Initial Program" results (Fig. 5) and the "Selected Geometry" results (Fig. 8). The most prominent difference is the centered saddle point at $x^* \approx 1.42$ for the former and the centered nodal point at $x^* \approx 1.2$ for the latter. Additionally, the distinct vortex cores are located at $x^* \approx 0.95$, $r^* \approx \pm 0.5$ for the former and (as noted above) $x^* \approx 0.9$ and $y^* \approx \pm 0.5$. The cross-member that is exposed to the annular jet flow was narrower ($\delta z/R_2=0.104$) in the earlier study cf. $\delta z/R_2=0.165$ for the "Selected Geometry". Also, the flow in the aft region of the plug (the "Initial Program") was clearly influenced by the interchangeable support structure. These geometric differences are the apparent cause for the flow field differences.

The aligned ($x-z$) plane velocity distribution (Fig. 9) is dramatically different than the $x-y$ plane velocity field. The distinct feature: the saddle point at $x^* \approx 1.12$, in this view is the nodal point in the perpendicular image (Fig. 8). The vortex cores (as identified by the centers of the tightly swirled streamlines) are positioned at much different locations for the aligned case. Namely, $x^* \approx 0.45$ and $z^* \approx \pm 0.28$. The x^* locations are similar to the values (0.48) in the Patte-Rouland, et al. [11] study. However the lateral positions are much different: ± 0.28 cf. ± 0.58 .

The ensemble mean velocity distribution can be further clarified by examining specific velocity distributions. Figure 10 shows the $\bar{u}(z^*)/U_o$ and the $\bar{u}(y^*)/U_o$ distributions at the x^* values that were investigated by Durao and Whitelaw [7]. That study's data are included for reference in Figs. (10-12). A striking result, as evidenced in these mean velocity data, is the influence of the thin ($\delta z/R_2=0.165$) support member.

The turbulence field properties: $\tilde{u}(z^*)/U_o$ and $\tilde{u}(y^*)/U_o$, as well as the respective negative kinematic Reynolds stresses, $\overline{u'w'}/U_o^2$ and $\overline{u'v'}/U_o^2$ have also been evaluated. Figures 11 and 12 present these results which are again compared with the available prior results.

The conventional understanding (for nominally parallel shear flows) that \tilde{u}^2 will be relatively large in regions of large production of turbulence kinetic energy (viz., where $\overline{u'v'}\partial\bar{u}/\partial y$ is large) is consistent with the present results.

The negative kinematic Reynolds stress ($\overline{u'v'}$) in the $x-y$ plane exhibits the "expected" feature that the peak values are in the regions of the strongest mean strain rates ($\partial\bar{u}/\partial y$). It is also

1. In keeping with the conference paper instructions, it is assumed that the reader has access to the "color" version of this paper.

of interest to note the weakly sheared regions along the primary jet column as well as the flow downstream of the nodal point ($x^* \geq 1.2$).

The experimental data for the aligned and the perpendicular traverses are, in general and as one could anticipate, quite different in character. One issue of similarity are the \bar{u} values except for the low values in the jet-like region of the perpendicular traverse (Fig. 11).

More informative comparisons can be formed using the perpendicular and the Durao, and Whitelaw [7] measurements referred to as D&W for convenience. The streamlined plug of the former leads to a relatively weak reverse flow: $\bar{u} = -0.23 U_o$ at $x^* = 0.6$ in contrast with the $-0.4 U_o$ value from D&W.

The streamwise intensity values (\bar{u}/U_o) for the present study are somewhat smaller than those for D&W at the first three x^* locations: 0.2, 0.6, and 1.3. Apparently, this is a result of the streamlined plug instead of the flat disk as used by those authors. A somewhat similar distribution is observed for $x^* = 2.16$. By implication, the D&W study involves larger production and dissipation of turbulence kinetic energy in the near field.

The negative kinematic Reynolds shear stress distributions reveal a much stronger interior (y^* , $r^* < 0.6$) stress field for the present study than that for the D&W investigation. Once again, this is an apparent result of the significantly different geometric configurations. One can note that the large shear stress values correlate well with respect to the large velocity gradient regions for the present data.

CONCLUSIONS

The objective of this investigation: "to determine the most appropriate diameter ratio to obtain a narrow jet field at $x/D_2 = 8$ with an adequate ratio of $Q(x/D_2 = 8)/Q(0)$ ", where (Q =flow rate), has resulted in the selection of $D_1/D_2 = 0.757$.

The $\delta z/R_2 = 0.165$ thick cross-member that supports the streamlined, elliptical nose plug in the second part of this study has a significant effect on the velocity field in the near-exit region: $0 \leq x^* \leq 2.5$. This is in contrast to the "sting supported plugs" reported in the literature which provide axisymmetric flows. It is also in contrast to the near field results for the thinner cross member ($0.104 R_2$); Figs 5 and 8 should be consulted to clarify these substantive differences. The Fig. 5 results are qualitatively similar to those of the axisymmetric geometry of Patte-Rouland, et al. [11].

Some of the specific differences between the aligned and the perpendicular geometries are:

- the centered saddle point in the x-z (aligned) plane in contrast with the centered nodal point in the x-y (perpendicular) plane.

- the common "vortex cores" are in strongly different positions for the two planes
- at the farthest downstream location: $x^* = 2.5$, the x-y (perpendicular) plane mean velocity distribution shows a "double peak" whereas the x-z (aligned) plane has a single peak.

REFERENCES

- [1] Rohles, F.H. (1981) "Thermal Comfort and Strategies for Energy-Conservation", *J Soc Issues*, **37**(2): 132-140.
- [2] Rohles, F.H., Konz, S.A. and Munson, D. (1982) "A New Psychometric Chart for Thermal Comfort", *ASHRAE J*, **29**(1): 85.
- [3] Brody, S., Ragsdale, A.C., Thompson, H.J. and Worstell, D. (1954) "The Effect of Wind on Milk Production, Feed and Water consumption and Body Weight in Dairy Cattle" *Mo. Agr. Exp. Sta. Res. Bull.* **545**, Univ. of Missouri, Columbia, MO.
- [4] Tyrrell, H.F., Brown, A.C.G., Reynolds, P.J., Haaland, G.C., Bauman, D.E., Peel, C.J. and Steinhour, W.D. (1988) "Effect of Somatotropin on Metabolism of Lactating Cows: Energy and Nitrogen Utilization as Determined by Respiration Calorimetry", *J. Nutr.* **118**:1024-1030.
- [5] Tillotson, R.J. and Bickert, W.G. (1994) "Dairy Housing Ventilation Modification Due to Level of Milk Production", in: *Dairy Systems for the 21st Century*, Proc. of the Third Int'l Dairy Housing Conf. ASAE, 2950 Niles Rd., St. Joseph, MI, pp. 317-326.
- [6] Chastain, J.P. (1991) "Heat and Mass Transfer Through the Bovine Hair Coat During Evaporative Cooling", unpublished PhD dissertation. University of Kentucky, Lexington, KY.
- [7] Durao, D.F.G. and Whitelaw, J.H. (1978) "Velocity Characteristics of the Flow in the Near Wake of a Disk", *J. Fluid Mech.*, **85**(2), pp. 369-385.
- [8] Ko, N.W.M. and Chan, W.T. (1978) "Similarity in the Initial Region of Annular Jets: Three Configurations", *J. Fluid Mech.*, **84**(4), pp. 641-656.
- [9] Ko, N.W.M. and Chan, W.T. (1979) "The Inner Regions of Annular Jets", *J. Fluid Mech.*, **93**(3), pp. 549-584.
- [10] Kuhlman, J. (1987) "Variation of Entrainment in Annular Jets", *AIAA Journal*, **25**(3), pp. 373-379.
- [11] Patte-Rouland, B., G. Lalizel, J. Moreau and E. Rouland (2001) "Flow Analysis of an Annular Jet by Particle Image Velocimetry and Proper Orthogonal Decomposition", *Meas. Sci. Tech.*, **12**, No. 9, September, pp. 1404-1412.

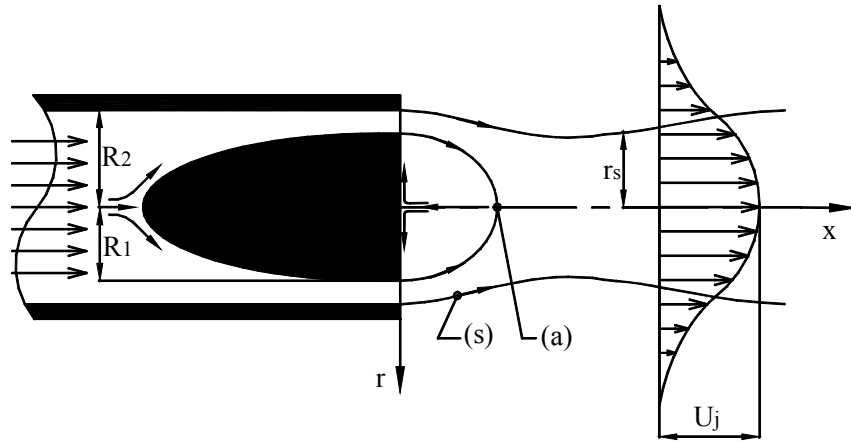


Figure 1. Conceptual representation of the annular exit geometry to achieve a narrowed jet column.

- Notes:**
- 1) (s) = separation stream surface
 - 2) (a) = aft stagnation point
 - 3) r_s = radius of separation stream surface
 - 4) U_j = centerline velocity of jet

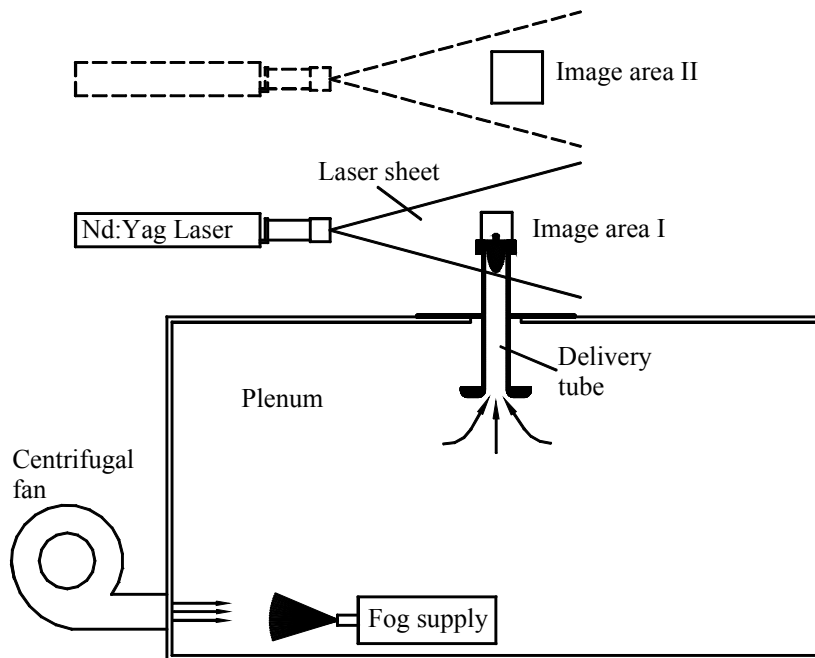


Figure 2. Experimental configuration for the initial jet studies.

- Notes:**
- 1) The data of Fig. 5 are from image area I.
 - 2) The data of Fig. 6 are from image area II.
 - 3) The geometry of Fig. 7, for the near field studies, was "flush mounted" at the top of the plenum.
 - 4) Fig. 7 shows the inlet nozzle for the "near exit" studies.

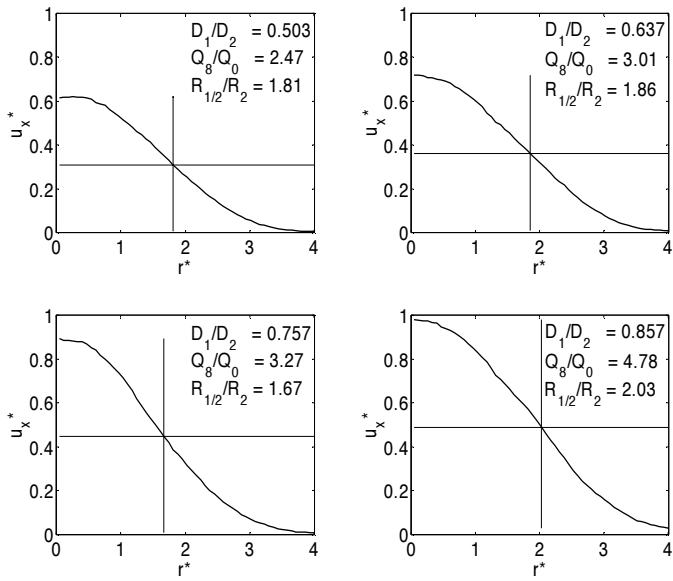


Figure 6. Initial study comparative mean velocity distributions at $x/D_2 = 8$ to define the "selected geometry" ($D_1/D_2 = 0.757$).

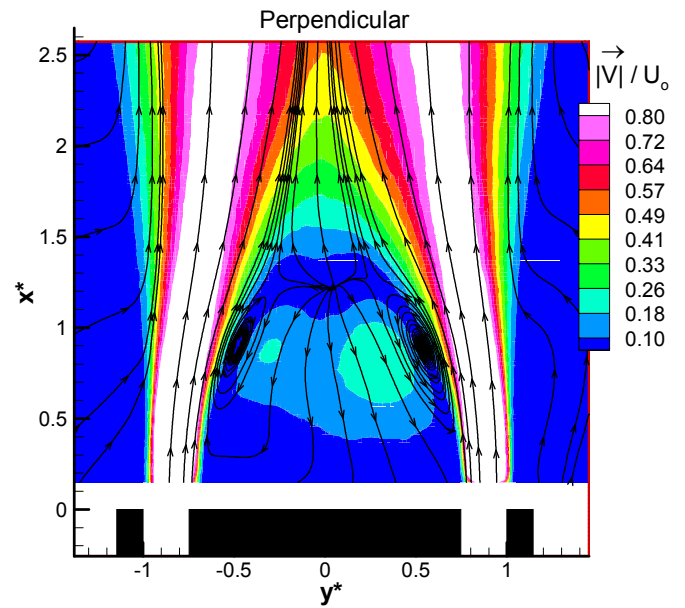


Figure 8. The near-field, perpendicular orientation, mean velocity field $|\vec{V}| = \sqrt{\vec{u}^2 + \vec{v}^2}$.

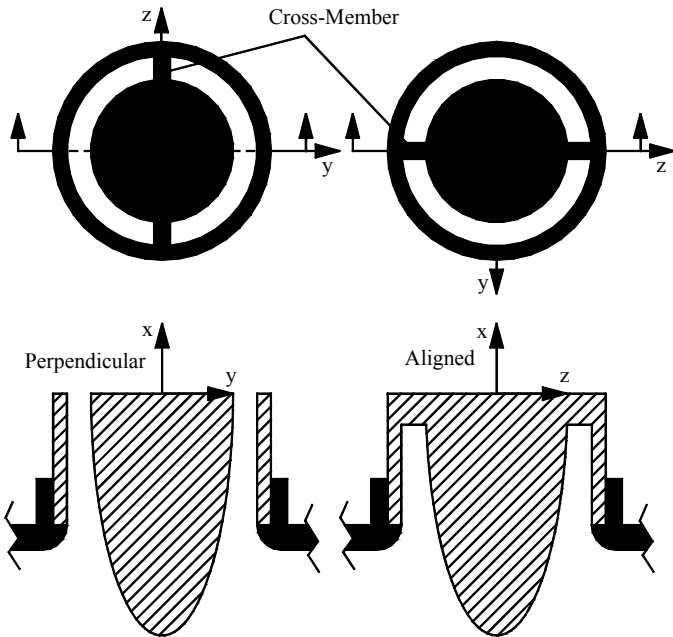


Figure 7. The selected geometry for the near-field investigation.

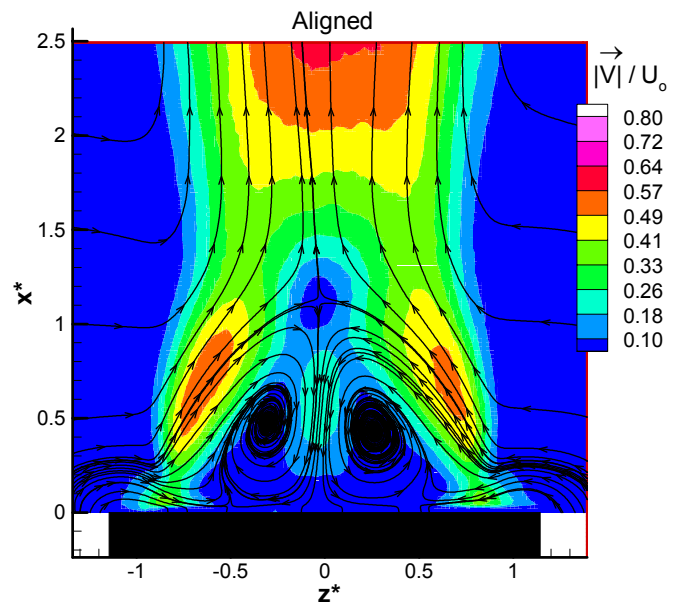


Figure 9. The near-field, aligned orientation, mean velocity field $|\vec{V}| = \sqrt{\vec{u}^2 + \vec{w}^2}$.

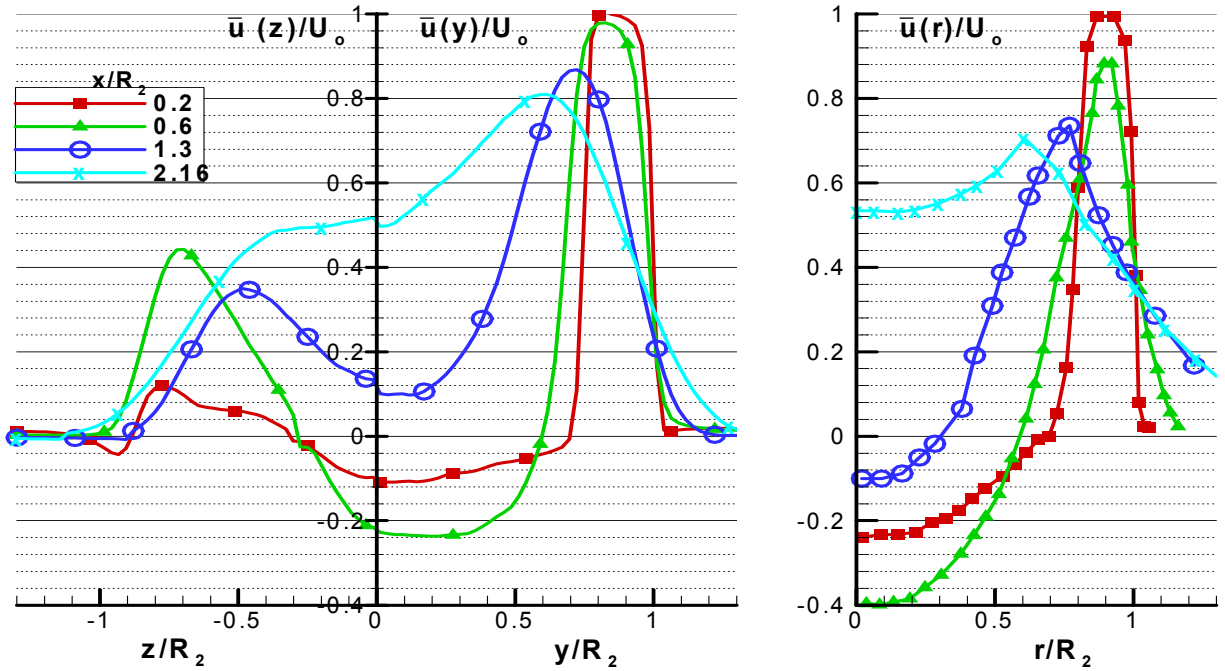


Figure 10. Comparative distributions of the axial velocity component for the aligned, the perpendicular and the experiment of Duraó and Whitelaw.

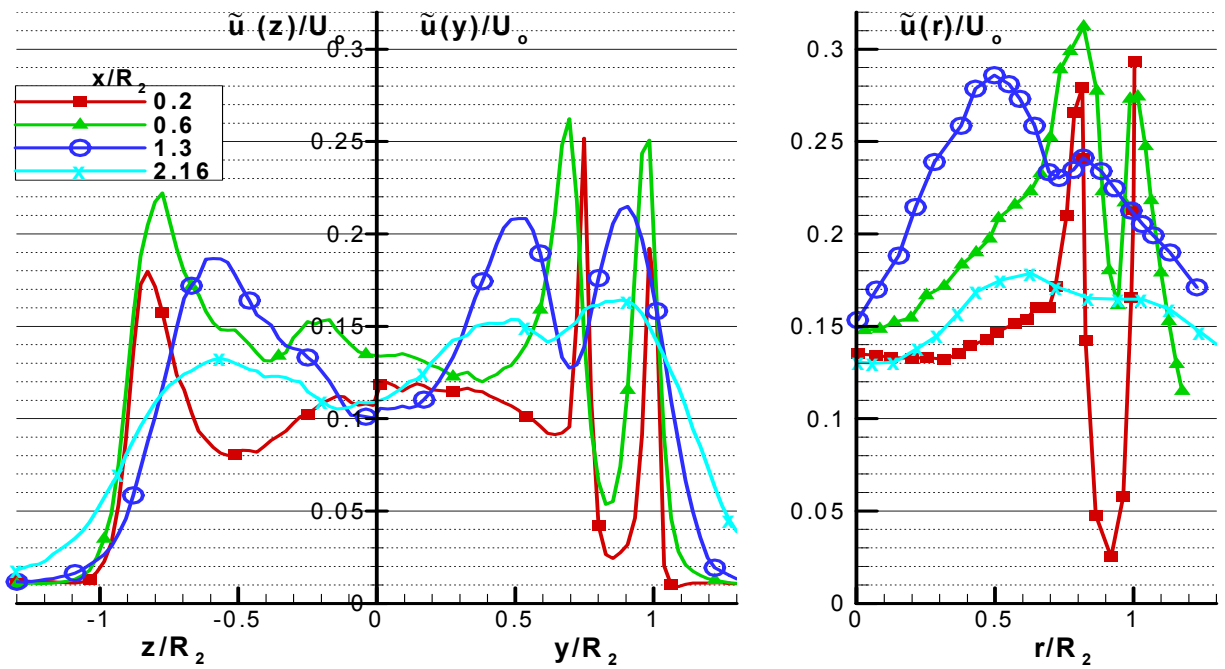


Figure 11. Comparative distributions of the axial fluctuation intensity values for the aligned, the perpendicular and the experiment of Duraó and Whitelaw.

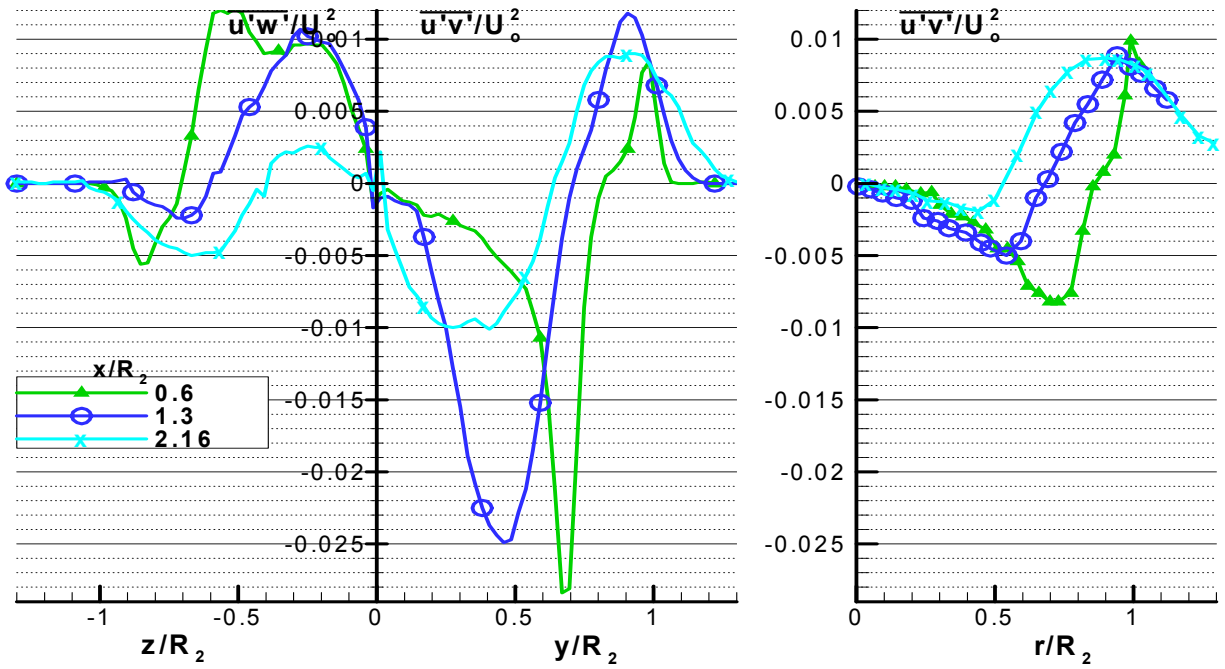


Figure 12. Comparative distributions of the negative kinematic Reynolds shear stress for the aligned, the perpendicular and the experiment of Durao and Whitelaw.